Food and Chemical Toxicology 133 (2019) 110778

Contents lists available at ScienceDirect

Food and Chemical Toxicology

journal homepage: www.elsevier.com/locate/foodchemtox

Structural characterization of a novel mannogalactoglucan from *Fortunella margarita* and its simulated digestion *in vitro*

Peilin Chen[a,c], Yan Lin[a], Yueyu Chen[a], Qing Chang[a,b], Baodong Zheng[a,b,c], Yi Zhang[a,b,c], Xiaoke Hu[d], Hongliang Zeng[a,b,c,*]

[a] College of Food Science, Fujian Agriculture and Forestry University, Fuzhou, Fujian, 350002, China
[b] Fujian Provincial Key Laboratory of Quality Science and Processing Technology in Special Starch, Fujian Agriculture and Forestry University, Fuzhou, 350002, China
[c] China-Ireland International Cooperation Centre for Food Material Science and Structure Design, Fujian Agriculture and Forestry University, Fuzhou, 350002, China
[d] Key Laboratory of Coastal Biology and Bioresource Utilization, Yantai Institute of Costal Zone Research, Chinese Academy of Sciences, Yantai, 264003, China

ARTICLE INFO

Keywords:
Polysaccharide fraction
Mannogalactoglucan
Fortunella margarita
Structural characterization
Simulated digestion

ABSTRACT

This study was to investigate the structure of a polysaccharide fraction from the *Fortunella margarita* and the relationship between its digestibility and structure. A novel polysaccharide fraction extracted by graded precipitation at ethanol concentrations of 20% from *F. margarita* (named FP20) comprised mainly glucose, galactose, and mannose. The unit composition was →4)-*β*-*Glcp*-(1 → 2)-*α*-*Glcp*-(1 → 2)-*α*-*Galp*-(1 → 4)-*α*-*Galp*-(1→ bone, and in →2)-*α*-*Galp*-(1→) with a branching point at C_6 of *β*-*Manp*. FP20 was identified as a mannogalactoglucan with a different monosaccharide composition ratio and side-chain sugar residues compared with other plant polysaccharides. Moreover, FP20 had a spherical aggregations by atomic force microscope test. FP20 had an island-shaped structures with a smooth surface revealed by field emission scanning electron microscopy. Furthermore, *in vitro* digestive test, FP20 was resistance to a digestion system of saliva-gastric-small intestinal. The digestibility of FP20 was related to its backbone unit, structure and tight, uniform, and spherical chain conformation in aqueous.

1. Introduction

Digestion starts in the mouth because of the action of α-amylase (Tenore et al., 2015) followed by gastric juice digestion, involving the digestive enzymes pepsin and gastric lipase (Pedersen et al., 2002). After digestion in the stomach, digestive products are further digested and absorbed by bile salts and enzymes in the small intestine (Cilla et al., 2009; Wen et al., 2015). Simulated digestion *in vitro* has been widely used to study the stability, bioactivity, and bioavailability of polysaccharides because of the simplicity, rapidity, and good reproducibility of this approach (Wang et al., 2018). Polysaccharides are one of the components in plant (Shi et al., 2016). In recent years, various studies have focused on the properties of polysaccharides during gastrointestinal digestion. For example, salivary amylase had no effect on mulberry fruit polysaccharides, whereas gastric enzymes had greater digestive effects on polysaccharide compared with intestinal enzymes (Chen et al., 2016). Liu et al. (2018) reported that salivary amylase had no effect on polysaccharides from the *Dendrobium aphyllum*, whereas these were digested by gastric-intestinal enzymes.

The *Fortunella margarita*, which originates from China, is a source of several nutritious bioactive compounds, including polysaccharides, limonoids, oils, flavonoids, and vitamins (Zeng et al., 2017). *F. margarita* polysaccharides comprised four polysaccharide fractions, comprising mainly galactose, galacturonic acid and mannose, and with β-glycosidic and α-glycosidic bonds (Zeng et al., 2016). These fractions display antioxidant and antibacterial activities, with inhibitory effects on pancreatic lipase, and strong bile acid-binding abilities (Zeng et al., 2016). Zeng et al. (2019) reported that *F. margarita* polysaccharides had a significant regulatory role in lipid metabolism disorder in hyperlipidemic rats. *F. margarita* polysaccharide fractions by graded ethanol precipitation could promote the proliferation of Gram-positive *Bifidobacterium in vitro*, especially a fraction obtained by graded precipitation

Abbreviations: (FP20), Polysaccharide fraction extracted by graded precipitation at ethanol concentrations of 20% from *Fortunella margarita*; (FTIR), fourier transform infrared spectroscopy; (GC), gas chromatography; (GC-MS), gas chromatography-mass spectrometry; (NMR), nuclear magnetic resonance; (AFM), atomic force microscope; (FESEM), field emission scanning electron microscope; (UV), Ultraviolet; (D2O), deuterium-oxide; (DSS), sodium dimethylsilopentane sulfonate; (SEC-MALLS-RI), size-exclusion chromatography, multi-angle laser light-scattering and refractive index

* Corresponding author. College of Food Science, Fujian Agriculture and Forestry University, Fuzhou, Fujian, 350002, China.
E-mail address: zhlfst@fafu.edu.cn (H. Zeng).

https://doi.org/10.1016/j.fct.2019.110778
Received 22 July 2019; Received in revised form 17 August 2019; Accepted 20 August 2019
Available online 28 August 2019

at ethanol concentrations of 20% (Chen et al., 2019). The intestinal activity of *F. margarita* polysaccharides *in vivo* might be related to their digestion and absorption characteristics in the oral cavity, stomach and small intestine. In addition, their digestion and absorption might also be impacted by their structure. Zhu et al. (2019a) reported that the antioxidant activity of polysaccharides from *Artocarpus heterophyllus Lam. (Jackfruit) Pulp* significantly increased after gastrointestinal digestion. Wang et al. (2015) reported that the digestion of polysaccharides was affected by their structure. Therefore, in the current study, we investigated the relationship between the structure of a polysaccharide fraction from *F. margarita* and the results of its simulated digestion *in vitro*.

To this end, a novel polysaccharide fraction was extracted from *F. margarita* by graded precipitation at ethanol concentrations of 20%. The fraction was characterized by fourier transform infrared spectroscopy (FTIR), gas chromatography (GC), gas chromatography-mass spectrometry (GC-MS), and nuclear magnetic resonance (NMR). The chain conformation and surface morphology were determined by atomic force microscope (AFM) and field emission scanning electron microscope (FESEM), respectively. Furthermore, the digestibility of the fraction in both a single and mixed digestive system was investigated.

2. Material and methods

2.1. Material and reagents

F. margarita was purchased from the Youxi Agricultural Bureau, Sanming City, Fujian Province, China. A polysaccharide fraction (named FP20) was prepared following the method of Chen et al. (2019). Briefly, fresh *F. margarita* was washed, crushed, extracted at 80 °C for 2 h, centrifuged, and precipitated with ethanol concentrations of 20% for 20 h at −4 °C. α-amylase, pepsin, gastric lipase, and trypsin were purchased from Beijing Solarbio technology Co., Ltd. (Beijing, China). KBr, dimethyl sulfoxide (DMSO), deuterium-oxide (D_2O), trifluoroacetic acid, hydroxylamine hydrochloride, pyridine, and NaOH were purchased from Shanghai Macklin biochemical technology Co., Ltd. (Shanghai, China), and all of them were chromatographic purity. Dichloromethane, Na_2HPO_4, KH_2PO_4, phosphate buffer, NaCl, KCl, $CaCl_2$, $NaHCO_3$, NaCl, acetic anhydride, P_2O_5, and iodomethane were purchased from China pharmaceutical group chemical reagents Co., Ltd. (Shanghai, China). Monosaccharide standards (ribose, arabinose, xylose, mannose, glucose and galactose) were purchased from sigma-Aldrich, Inc. (USA).

2.2. Ultraviolet (UV) and FT-IR spectra analysis

FP20 was prepared as a 1 mg/mL solution with distilled water and scanned in the whole band of ultraviolet–visible spectrum in the wavelength range of 200–800 nm (Tang et al., 2017) with a scanning interval of 1 nm using a Thermo Scientific Nano Drop 2000/2000c (Massachusetts, USA).

The polysaccharide and KBr solution was dried in an oven (60 °C, 12 h) and free water was removed to eliminate the interference of water molecules with absorption peaks. The powder was weighed out into 2-mg aliquots and placed in an agate mortar, to which ~400 mg of dry KBr was added. The powder was ground uniformly under the infrared lamp (Tianjin Energy Spectrum Technology Co., Ltd., China). The powder was put into a pressing die and vacuum pressed into thin sheets. FT-IR of Nicolet AVATAR360 (Madison, Wisconsin, USA) was used to scan polysaccharide sample. The scanning wavelength ranged from 400 to 4000 cm^{-1}, the scanning times were 24 times, and the resolution was 4 cm^{-1} (He et al., 2007).

2.3. Determination of monosaccharide composition

3–5 mg FP20 was hydrolyzed with 2 mL 2 M trifluoroacetic acid at 95 °C for 4 h in an ampoule bottle, and dried with N_2 at 70 °C (Yu et al., 2017; Zhang et al., 2017). Then, 10 mg hydroxylamine hydrochloride and 0.5 mL pyridine were added to the hydrolysate and monosaccharide standard, respectively and reacted in a water bath at 90 °C for 30 min. After cooling to room temperature, 0.5 mL acetic anhydride was added to the hydrolysate, and further reacted in a water bath at 90 °C for 30 min. Derivatives were obtained through a 0.45 μm organic system filter membrane. Gas chromatography (Agilent 7890A, Palo Alto, California, USA) with a capillary column, HP-INNOWAX (30 m × 0.32 mm × 0.25 μm) was used to determine the monosaccharide content and was run at 170 °C for 2 min to 250 °C for 15 min at a heating rate of 10 °C/min, using N_2 as carrier gas at 30 mL/min, H_2 as a fuel gas at 30 mL/min, and air as an auxiliary gas at 30 mL/min at a ratio of 40:1.

2.4. Methylation and GC–MS analysis

Methylation was determined by the method according to Gong et al. (2015), with minor modifications. Polysaccharide sample (~10 mg) was placed in a 25-mL round-bottomed flask, sealed with a sealing film, with a few holes, dried in a vacuum dryer with P_2O_5 (60 °C, 24 h), and treated overnight. Then, 2 mL dry DMSO was added to the bottle, which was sealed with a rubber plug covered with sealing film. The bottle was treated with ultrasound at 50 °C for 6.5 h and then placed in a water bath at 85 °C for 120 r/min for 2 h. Then, it was stirred at room temperature overnight. Preground and dried NaOH powder (20–30 mg; previously dried in a vacuum dryer) was then added to the flask and stirred for 2 h at room temperature to obtain a yellow-colored solution, followed by the addition of 0.5 mL iodomethane and stirring at room temperature for 2.5 h. The reaction was terminated by adding 1 mL distilled water and 1 mL dichloromethane to extract the methylation product. The solution was dried with N_2 by Termovap Sample Concentrator (HNDK400, Shanghai Hannuo Instruments Co., Ltd., China) to obtain the methylation products.

The methylated product was analyzed using a GC-MS TQ8040 (Shimadzu GC-2010, Japan) with a RTX-5 capillary column (30 m × 0.25 mm × 0.25 μm) (Shimadzu, Japan), run at 170 °C for 2 min to 250 °C for 15 min at a heating rate of 10 °C/min, and then heating to 300 °C at a heating rate of 20 °C/min, using He_2 as a carrier gas. The injector temperature was 260 °C, the ion source temperature was 180 °C, and the voltage was 70 eV. The multiplier voltage was 350 V and the filament current was 250 A, in the scanning range of 30–450 m/z.

2.5. Nuclear magnetic resonance (NMR) spectroscopy

30-mg sample of FP20 was weighed into a NMR tube, and a 4.0% solution (W/V) was prepared by adding D_2O. The ^1H and ^{13}C spectra were analyzed by using an AVANC III 500 NMR spectrometer (Bruker, Switzerland). Sodium dimethylsilopentane sulfonate (DSS) was used as an internal standard, and the test temperature was set at 35 °C. ^1D NMR (^1H NMR and 13C NMR) and ^2D NMR (COSY, TOCSY, NOESY, HSQC, and HMBC) were measured (Ye et al., 2011).

2.6. Atomic force microscope (AFM) microscopy

The ultrastructure of FP20 was analyzed by AFM (Agilent, Palo Alto, California, USA). A sample of FP20 was prepared as a 1 μg/mL solution with ultrapure water. 5 μg/mL sample was dried on fresh mica sheets under N_2 and then scanned by using AFM.

2.7. Field emission scanning electron microscopy (FESEM)

The microstructure of FP20 was determined by using FESEM (Nova Nano SEM 230, FEI Czech Republic S.R.O. CA., Czech). FP20 powder samples were adhered to the sample table, and platinum (Pt) was

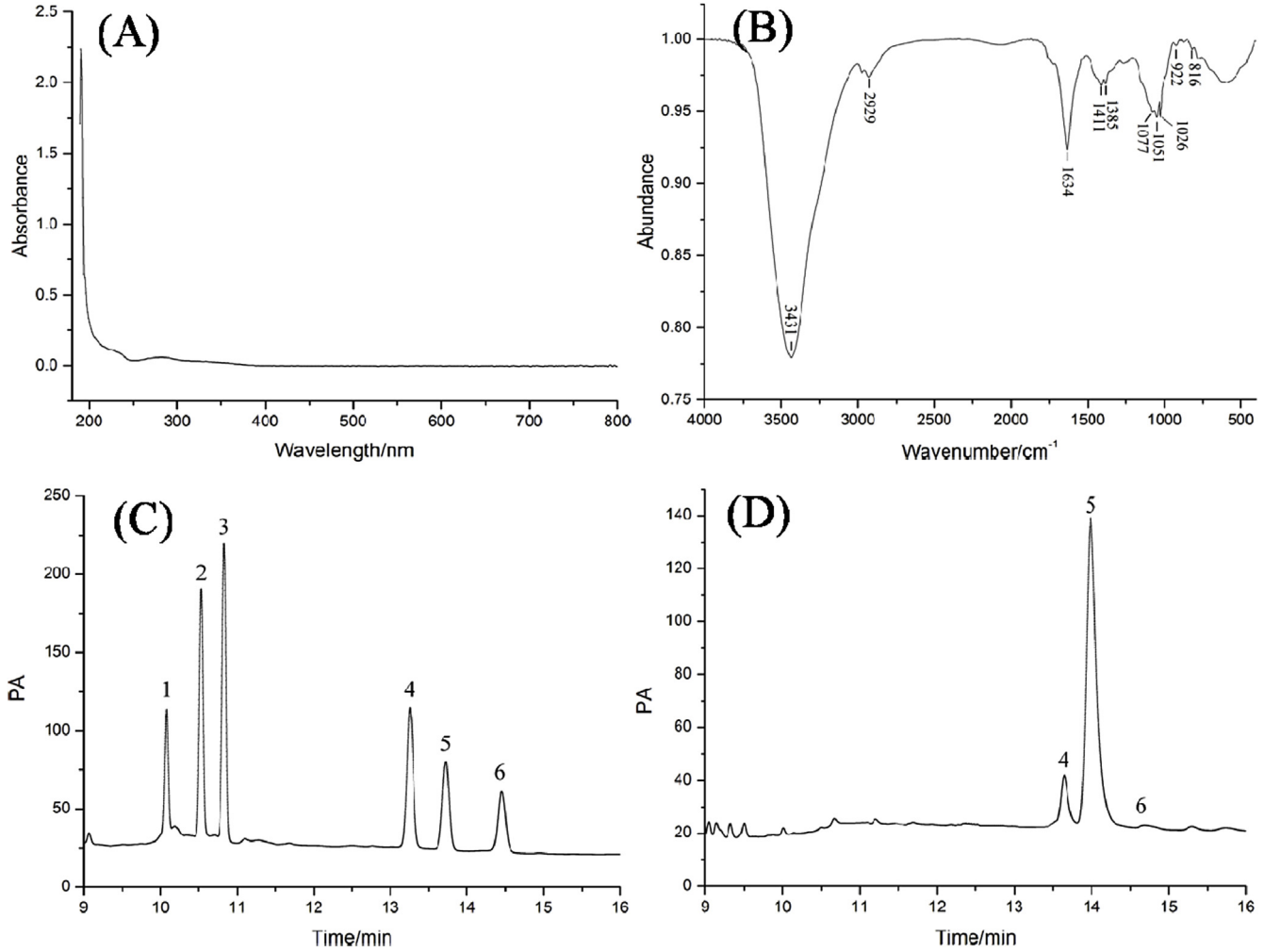

Fig. 1. Scanning spectra of FP20 by using ultraviolet–visible light spectrophotometer (A), FT-IR spectra of FP20 (B), monosaccharide mix reference material GC chromatography (C), and monosaccharide composition GC chromatography of FP20 (D).

deposited using a vacuum sprayer to a thickness of 10 nm. The acceleration voltage of the electron gun was 15 keV. The sample was magnified to 500 × , 1000 × , 2000 × , and 5000 × .

2.8. In vitro digestion and determination of molecular weight

2.8.1. Simulated saliva digestion

Saliva was prepared according to the method of Humphrey and Williamson, (2001) , with slight modifications. 2.38 g Na_2HPO_4, 0.19 g KH_2PO_4, 8.00 g NaCl, and 0.91 g α-amylase (220 U/mL) were dissolved in 1 L water to form simulated saliva. The pH of the solution was adjusted to 6.75 with phosphate buffer. FP20 was added to the simulated saliva juice at a concentration of 2.0 mg/mL, to form the test group. The control group contained only saliva juice. Three samples of each group were tested. All the samples were incubated at 37 °C in a shaking water bath at 150 r/min. After digestion for 2, 4, and 6 h, the samples were boiled in water for 20 min to stabilize the enzymes.

2.8.2. Simulated gastric digestion

Gastric juice was prepared according to the method of Yun et al. (2019). A gastric electrolyte solution (1000 mL) was prepared with 3.10 g NaCl, 1.10 g KCl, 0.15 g $CaCl_2$, and 0.60 g $NaHCO_3$. Then, 135 mg pepsin and 119 mg gastric lipase were added to 180 mL of the gastric electrolyte solution. The pH value was adjusted to 2.00 with 0.1 M HCl. FP20 was added to the simulated gastric juice at a concentration of 2.0 mg/mL, to form the test group. The control group contained only gastric juice. Three samples of each group were tested. All samples were incubated at 37 °C in a shaking water bath at 150 r/min. After digestion for 2, 4, and 6 h, they were boiled in water for 20 min to stabilize the enzymes and neutralized with 1.0 M $NaHCO_3$.

2.8.3. Simulated small intestinal digestion

Intestinal juice was prepared according to the method of Zheng et al. (2010). The intestinal electrolyte solution (1000 mL) comprised 5.40 g NaCl, 0.65 g KC1, and 0.33 g $CaCl_2$. 7.00 g trypsin was dissolved in 100 mL water and centrifuged at 4800 r/min for 10 min. The supernatant was then removed. 90 mL of the trypsin solution was added to 90 mL of the intestinal electrolyte solution. The pH was adjusted to 7 with 1.0 M $NaHCO_3$. FP20 was added to the simulated intestinal juice at a concentration of 2.0 mg/mL, to form the group. The control group contained only small intestinal juice. Three samples of each group were tested. All samples were incubated at 37 °C in a shaking water bath at 150 r/min. After digestion for 2, 4, and 6 h, they were boiled in water for 20 min to stabilize the enzymes.

2.8.4. Simulated saliva-gastric and saliva-gastric-small intestinal digestion

The solution that remained after the simulated saliva digestion was mixed with the gastric juice in a ratio of 2:1. The resulting solutions were further incubated at 37 °C in a shaking water bath at 150 r/min for 6 h, boiled in water for 20 min to stabilize the enzymes and neutralized with 1.0 M $NaHCO_3$.

The solution that remained after simulated saliva-gastric digestion

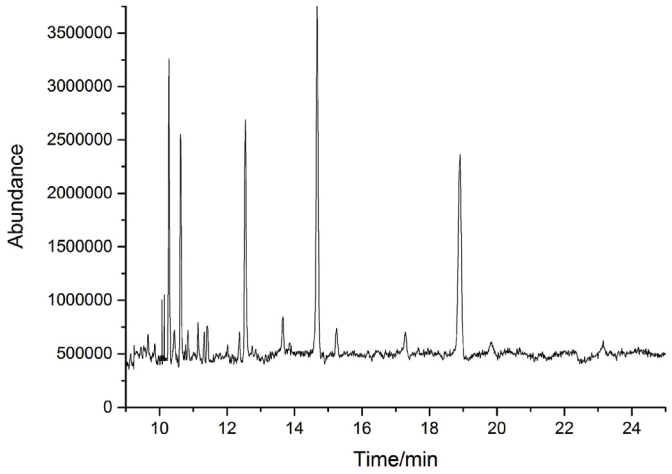

Fig. 2. GC-MS total ion chromatogram of FP20.

was mixed with the small intestinal juice in a ratio of 2:1. The resulting solutions were further incubated at 37 °C in a shaking water bath at 150 r/min for 6 h, boiled in water for 20 min to stabilize the enzymes.

2.8.5. Determination of molecular weight

The molecular weight of FP20 was determined by using size-exclusion chromatography, multi-angle laser light-scattering and refractive index (SEC-MALLS-RI) (Wyatt Technology, CA, USA), according to the method of Zeng et al. (2015), with slight modifications. The mobile phase was a 0.10 mol/L NaCl solution at a flow rate of 0.50 mL/min with an SB-806 column and a SB-803 column (Shodex, Tokyo, Japan) at 25 °C.

2.9. Statistical analysis

All figures were drawn using Origin 8.0 (Origin Lab Corporation, Northampton, MA, USA). The data obtained by FT-IR were analyzed by OPUS Spectroscopy Software. The data obtained by NMR were analyzed by Mest Re Nova statistical method. The data obtained by SEC-MALLS-RI was analyzed by ASTRA 6.1 sofware (Wyatt Technology, CA, USA).

3. Results and discussion

3.1. Purity, FT-IR spectra and monosaccharide composition analysis

The results of the UV spectroscopy was shown in Fig. 1A and contained no obvious peaks at 260–280 nm, indicating no nucleic acids or proteins in the samples. Ji et al. (2019) reported that there was no absorption at 260–280 nm of a polysaccharide fraction (PZMP2-2) from *Ziziphus jujuba* cv. *Muzao*, which also suggested that no nucleic acids or protein were present in the sample. Our previous study (Chen et al., 2019) reported that FP20 had a single, symmetrical peak based on the results of gel permeation chromatography, indicating the high purity of FP20.

As shown in Fig. 1B, the FT-IR spectra of FP20 had absorption in bands at 3431, 2929, 1634, 1411, 1385, 1077, 1051, 1026, 922, and 816 cm^{-1}, which were typical bands of carbohydrates (range 4000–400 cm^{-1}). The wide band at 3431 cm^{-1} was likely to be the result of O–H stretching vibration of hydrogen bonds within or between sugar molecules, whereas that at 2929 cm^{-1} was likely to be the result of C–H stretching vibrations in methylene (–CH_2–) (Zeng et al., 2016). The band at 1634 cm^{-1} was characteristic of intramolecular hydrogen bonds (Li et al., 2017a). Absorption bands at 1411 cm^{-1} and 1385 cm^{-1} represented CH_2 bending (Zhu et al., 2019b). There were three absorption bands in the range of 1100–1010 cm^{-1}, representing pyranose rings (Yang and Zhang, 2009). Bands that appeared at 1077 cm^{-1}, 1047 cm^{-1} and 891 cm^{-1} might be attributed to β-glycosidic linkage presence. A weak band at 918 cm^{-1} could be attributed to the deformation scissor vibrations of (CHH) and (COH) bonds (Ognyanov et al., 2018). The characteristic absorption bands at 816 cm^{-1} indicated that FP20 contained α-glycosidic linkages (Yu et al., 2015).

The monosaccharide composition of FP20 was identified by GC using an external standard method for comparison with retention time. The GC result of monosaccharide standards and monosaccharide composition of FP20 were shown in Fig. 1C and Fig. 1D, respectively. In Fig. 1C, numbers 1–6 represent ribose, arabinose, xylose, mannose, glucose, and galactose, respectively. Thus, FP20 comprised three monosaccharides (glucose, mannose, and galactose), with relative molar ratios of 48.56%, 14.97%, and 36.47%, respectively. The monosaccharides were similar to those reported by Colodel et al. (2018), who reported that the cell wall polysaccharide fraction HB_4 from ponkan peel contained glucose, galatose, and mannose, which was a type of galactoglucomannan. While polysaccharides from commercial carob flour mainly comprised mannose and galactose with minor glucose, which was a typical galactomannan (Petkova et al., 2017).

3.2. Methylation analysis

The GC-MS total ion chromatogram of FP20 is detailed in Fig. 2 and shows five peaks. Based on the relative retention time and the pyrolysis rule of polysaccharides, fragment plasmid-nucleus ratio and spectrogram library, these five peaks were analyzed, and the methylation analysis results are shown in Table 1. The peaks in Fig. 2 were identified as 2,3,4,6-Me_3-mannitol, 2,3,6-Me_3-glucitol, 2,3,6-Me_3-galactitol, 3,4,6-Me_3-glucitol, and 3,4-Me_2-galactitol, with percentages of 14.44%, 12.19%, 16.68%, 31.34%, and 25.35%, respectively. The data from the methylation analysis suggested that FP20 comprised three monosaccharides, in accordance with the GC results, and had a five-sugar residue comprising *Manp* linked T→ glucosidic bands, *Glcp* linked 1 → 2 or 1 → 4 glucosidic bands, and *Galp* linked 1 → 2 or 1 → 4 glucosidic bands, indicating that these monosaccharides were pyranose, consistent with the result of FT-IR. Nei et al. (2011) reported that *Cordyceps sinensis* polysaccharide was mainly comprised of 1 → 4 links and T→ links, but without 1 → 2 links. However, Zhang et al. (2010) reported 1 → 3 linked, 1 → 2 linked, and 1 → 4 linked polysaccharide from *Lentinus edodes*.

3.3. ^{1} D, and ^{2} D NMR analysis

The structural characterization of FP20 was further elucidated by ^{1} D, and ^{2} D NMR spectral analysis. Signals in the 4.5–5.0 ppm range in the ^{1} H NMR spectrum indicated that the polysaccharide had a *β*-glycosidic configuration, whereas those in the 5.0–5.5 ppm range indicated an *α*-glycosidic configuration. As shown in Fig. 3A, the chemical shifts at 5.31, 5.30, 5.11, 4.70, and 4.53 ppm in the ^{1} H NMR spectrum indicated that FP20 contained both *α*- and *β*-glycosidic configurations, in agreement with the results of FT-IR and GC-MS. The anomeric proton signal at 4.77 ppm was consistent with the presence of mannopyranosyl

Table 1
Methylation analysis and mode of linkage of FP20.

Retention time (min)	Methylated sugar	Linkage	Peak area percentage (%)
10.28	2, 3, 4, 6-Me_3-mannitol	T-	14.44
10.62	2, 3, 6-Me_3-galactitol	1, 4-	12.19
12.54	2, 3, 6-Me_3-glucitol	1, 4-	16.68
14.67	3, 4, 6-Me_3-glucitol	1, 2-	31.34
18.92	3, 4-Me_2-galactitol	1, 2, 6-	25.35

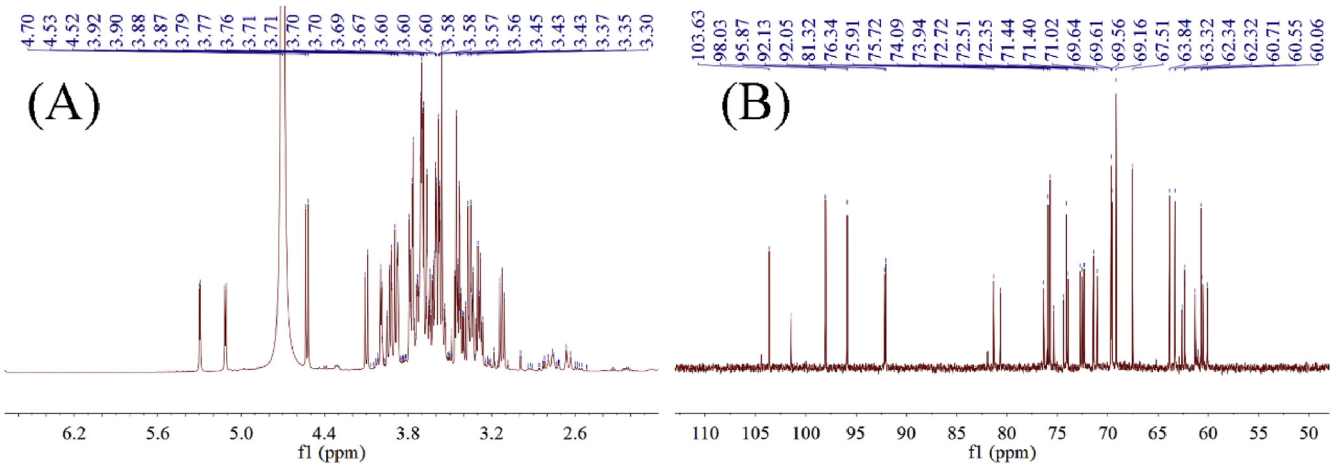

Fig. 3. ^{1}H (A) and ^{13}C (B) NMR spectra of FP20.

residues and that at 4.52 ppm was characteristic of glucopyranosyl residues (Xue et al., 2012). By comparison with the results of GC-MS, peaks at 4.70 ppm and 4.53 ppm could be attributed to *T-Manp* and 1,2-*Glcp* or 1,4-*Glcp*. Generally, the signal of *β*-hetero-protons was 0.3–0.5 ppm lower than that of α-hetero-protons (Cheng and Neiss, 2012; Nie et al., 2011; Yang and Zhang, 2009), suggesting that the peak at 5.11 ppm was *α-Glcp*. Feng et al. (2018) reported that the proton signal at 5.19 ppm was *α-Glcp*. The signals at 90–110 ppm indicated heterotopic carbon resonance. As shown in Fig. 3B, there were five signals in the ^{13}C NMR spectrum at 103.63, 98.03, 95.87, 92.13, and 92.05 ppm. The peak at 92.13 and 92.05 ppm could be assigned to α-galactose, in accordance with the study by Zhang et al. (2018), who reported that a peak at 93.15 ppm indicated the presence of C1 of the α-galactose.

H_2, H_3, H_4, H_5, and H_6 signals were assigned by combining the data from COSY (Fig. 4A), NOESY (Fig. 4B), and TOCSY (Fig. 4C), and the correlating proton and carbon (H_1/H_2, H_2/C_2, H_3/C_3, H_4/C_4, H_5/C_5, and H_6/C_6) signals were found in HSQC. All ^{1} H and ^{13} C signals were shown in Table 2A. The peaks in the region of 3.11–3.92 ppm were the signal characteristics of H_2–H_6 (Chen et al., 2018b; Cheng and Neiss, 2012). According to HSQC (Fig. 4D), the correlating anomeric proton and heterotopic carbon signals were found at δ H/δ C 5.31/92.13 and 5.30/92.05 indicated the presence of *α-Galp* (named residue A and B). The correlating chemical shift at δ H/δ C5.11/103.63 was assigned to *α-Glcp* (named residue C). The cross peak at δ H/δ C4.70/95.87 was characteristic of *β-Manp* (named residue D). The cross peak at δ H/δ C4.53/98.03corresponded to *β-Glcp* (named residue E). The peaks in the region of 96.62–60.06 ppm showed the signal characteristics of C_2–C_6 (Zhao et al., 2016). There was no signal in the region of 82–88 ppm, indicating that the sugar residue was a pyranose ring (Fan et al., 2006), consistent with the result of GC-MS.

The sequences of glycosyl residues in FP20 were identified by a HMBC (Fig. 4E), and the results are shown in Table 2B. According to previous studies (Chen et al., 2018b; Cheng and Neiss, 2012; Li et al., 2017b; Liu et al., 2016; Zhao et al., 2016), the possible sugar residue links of FP20 were as follows: residues A had an δ H signal at 5.31 ppm, and a δ C chemical shift at 72.72 and 73.07 ppm, indicating that residues A were interconnected with residues B and D by α-1→4. Residue B was α-1→4 linkage residue E supported by a δ H chemical shift at 5.30 ppm and a δ C signal at 73.07 ppm. Residue C was α-1→2 linkage residue A supported by a δ H chemical shift at 5.11 ppm and a δ C signal at 71.40 ppm. Residue D was assigned to be a nonreducing end mannose unit, connected with residue A by C_6 with β-1→6. The cross-peak at δ4.53/δ75.91 showed that the H-1 of residue E was correlated to the C-2 of residue C, indicating that the glucose was attached to the →2)-*α-Glcp*-(1→ residue. The repeating unit of FP20 was established based on the FT-IR, GC-MS, ^{1} D, and ^{2} D NMR results (Fig. 5). Thus, FP20 was characterized as a type of mannogalactoglucan, comprising →4)-*β-Glcp*-(1 → 2)-*α-Glcp*-(1 → 2)-*α-Galp*-(1 → 4)-*α-Galp*-(1→ bone, and →2)-*α-Galp*-(1→ with a branching point at C_6 of *β-Manp*. Schroder et al. (2001) reported that kiwifruit galactoglucomannan contained *Gal–Glc–Man* in the ratio of 1:2:2, which was different with our result of the *Gal–Glc–Man* ratio. Capek et al. (2000) reported that the side-chains terminated at position O-6 were predominantly D-galactose units in galactoglucomannan from the secondary cell wall of *Picea abies L. Karst*, whereas, in our study, the side-chains was β-mannan at the O-6 position of →2)-*α-Galp*-(1 → .

3.4. AFM analysis

AFM is an effective method to observe the chain conformation of macromolecules, such as polysaccharides and proteins (Wang et al., 2014). The chain conformations of polysaccharides involve spheres, random linear chains, and random chains with branches and rods. Chain conformations determined by AFM was generally consistent with those determined by other tools, such as SEC-MALLS-RI. Li et al. (2017b) reported that the chain conformation of sulfated polysaccharides from sea cucumbers determined by AFM were consistent with the results of SEC-MALLS-RI. The AFM image of FP20 was shown in Fig. 6. FP20 had several aggregates in the range of 9 μm × 9 μm (Fig. 6A. The range of 0.8 μm × 0.8 μm (Fig. 6B) indicated a single FP20 aggregate. The AFM results indicated that FP20 showed a spherical aggregation, consistent with a previous result based on SEC-MALLS-RI (Chen et al., 2019). This might be because FP20 molecules are intertwined, which could be a result of the structure unit of FP20 with a branching and strong intramolecular and intermolecular interactions resulting from hydroxyl groups (Giannotti et al., 2007; Liu et al., 2016).

3.5. FESEM analysis

The surface morphology of FP20 was determined by FESEM. Fig. 7 shows images at a magnification of 500×, 1000×, 2000×, and 5000×. The units of FP20 were tightly aggregated, consistent with a previous study of okra polysaccharides (Gao et al., 2018). At a magnification of 500× (Fig. 7A), the FP20 units entangled in large quantities and morphed into a circular aggregated mass, which was consistent with the result of AFM. At a magnification of 1000×, there were some island-shaped structures with a smooth surface (circled in Fig. 7B), and some random cross-networked structures (arrows in Fig. 7B). At a magnification of 2000×, there was a layered structure at the bottom of an island structure (arrow in Fig. 7C). At a magnification

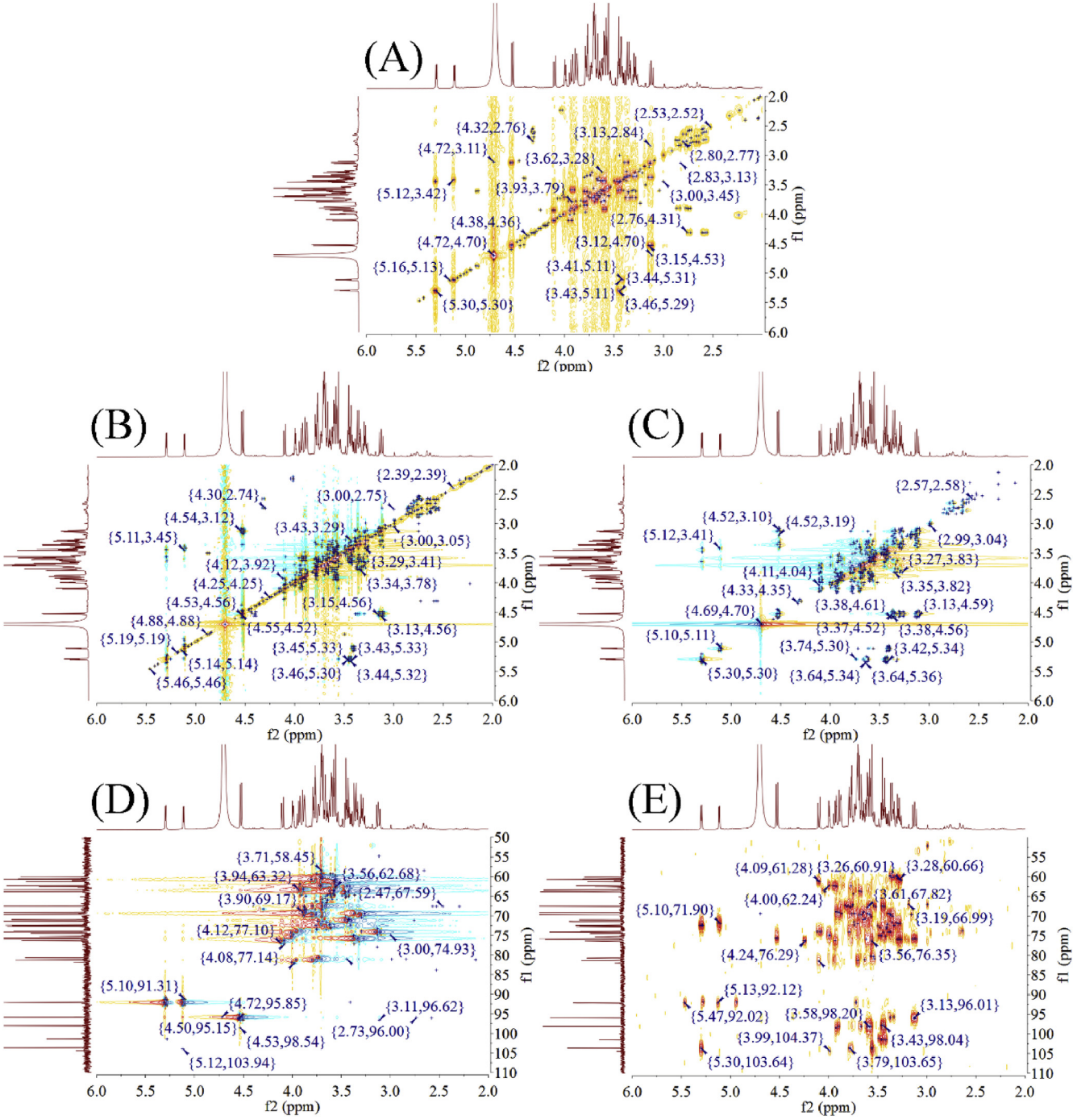

Fig. 4. ^{1} H/^{1}H COSY (A), ^{1}H/^{1}H NOESY (B), ^{1}H/^{1}H TOCSY (C), HSQC (the correlating proton and carbon) (D) and ^{1}H/^{13}C HMBC (E) NMR spectra of FP20.

Table 2a
NMR data for FP20(a): The detailed ^{1}H and ^{13}C NMR spectral assignments of FP20.

	H1/C1	H2/C2	H3/C3	H4/C4	H5/C5	H6/C6
A	5.31/92.13	3.44/71.40	3.58/64.77	3.67/72.72	3.80/67.52	3.32/69.64
B	5.30/92.05	3.51/63.87	3.60/65.16	3.68/72.67	3.59/61.29	3.26/73.95
C	5.11/103.63	3.38/75.91	3.72/71.33	3.29/73.94	3.62/63.84	3.92/62.32
D	4.70/95.87	3.11/96.62	3.37/77.17	3.65/72.67	3.46/71.04	3.59/59.32
E	4.53/98.03	3.13/77.98	3.36/69.37	3.63/73.07	3.77/72.43	3.57/59.66

Table 2b
The significant connectivities observed in ^{1}H-^{13}C HMBC for anomeric H/C of sugar residue of FP20.

Residues	H1/C1 δ H/δ C	Observed connectivities		
		δ H/δ C	Residues	Atom
A: →2, 6)-α-Galp-(1→	5.31	72.67	B	C-4
		73.07	D	C-4
B:→4)-α-Galp-(1→	5.30	73.07	E	C-4
C: →2)-α-Glcp-(1→	5.11	71.40	A	C-2
D: β-Manp-(1→	4.70	69.64	A	C-6
E: →4)-β-Glcp-(1→	4.53	75.91	C	C-2

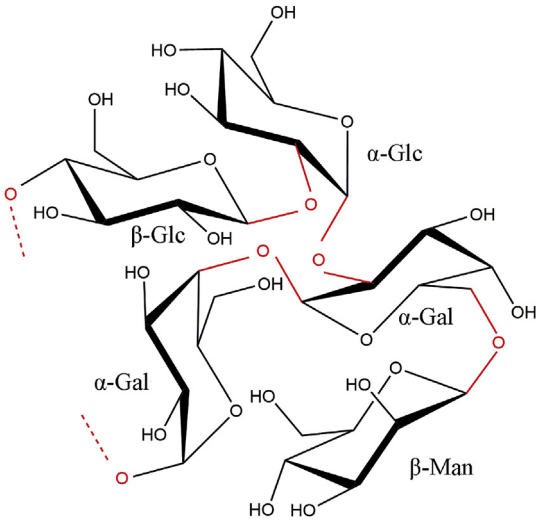

Fig. 5. Chemical structure unit of FP20.

of 5000×, there were some bores in the island structure (circled in Fig. 7D). Huo et al. (2019) reported that an exopolysaccharide from *Lachnum* was a block with a smooth surface. The surface of *Inonotus obliquus* polysaccharide was also smooth (Ma et al., 2012), consistent with our result.

3.6. Simulated digestion in vitro

3.6.1. Simulated saliva, gastric, and small intestinal digestion

In simulated saliva, α-amylase can act on α-(1 → 4)-linkage in carbohydrates, including starch and some non-starch polysaccharides (Pedersen et al., 2002). The molecular weight of FP20 after digestion *in vitro* is shown in Table 3. According to our previous study, the molecular weight of FP20 was ~1.341×10^6 g/mol. After simulated saliva digestion for 2, 4, and 6 h, the molecular weights of FP20 were 1.253×10^6 (± 1.579%), 1.261×10^6 (± 1.778%), and 1.212×10^6 (± 2.972%) g/mol, respectively. These results suggested that FP20 could not be digested by saliva, in agreement with previous study. Di et al. (2018) reported that the molecular weight of sulfated polysaccharides from *Gracilaria rubra* did not change significantly after saliva digestion. This might be related to the chain conformation of FP20 in aqueous solution, which displayed a tight, uniform, spherical conformation. It might also be because of the structure of FP20, with its backbone formed by →4)-*β-Glcp*-(1 → 2)-*α-Glcp*-(1 → 2)-*α-Galp*-(1 → 4)-*α-Galp*-(1→ repeats, with alternating →2)-*α-Galp*-(1→ with a branching point at C_6 of *β-Manp*, in accordance with previous study. Ding et al. (2018) reported that *Lycium barbarum* polysaccharide could not be digested by saliva, which might be related to its structure with a backbone formed by →4-*α-GalpA*-(1→, repeats, and a partial region connected by alternating →4)-*α-GalpA*-(1→ and →2)-*α-Rhap*-(1→).

After simulated gastric digestion for 2, 4, and 6 h, the molecular weights of FP20 were 1.284×10^6 (± 1.538%), 1.157×10^6 (± 2.579%), and 1.099×10^6 (± 1.480%) g/mol, respectively (Table 3). Compared with the initial molecular weight, there was no significant difference following simulated gastric digestion, indicating the resistance of FP20 to digestion by gastric juice, in accordance with previous studies. Chen et al. (2018a) reported that the molecular weight of Fuzhuan brick tea polysaccharide did not change in response to simulated gastric digestion. This might be because of the structure of FP20, which was composed with mannose, galactose, and glucose. Wang et al. (2015) reported that synthetic galactoglucomannan, comprising mannose, galactose, and glucose, was less susceptible to gastric juice digestion, even after 4 h at pH 1.5.

After simulated small intestinal digestion for 2, 4, and 6 h, the molecular weights of FP20 were 8.415×10^5 (± 1.381%), 3.413×10^5 (± 3.289%), and 3.130×10^5 (± 1.457%) g/mol, respectively (Table 3). Thus, the molecular weight of FP20 had decreased, indicating that FP20 was susceptible to digestion by small intestinal juice, possibly because enzymes in the small intestinal was able to

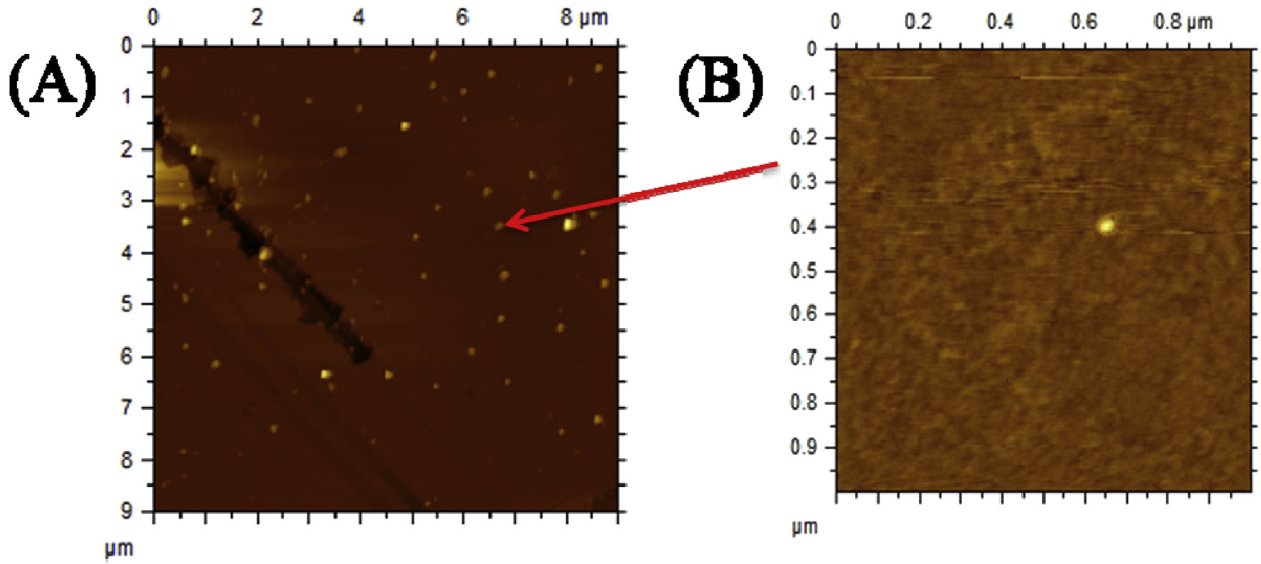

Fig. 6. Scanning atomic force microscope of FP20.

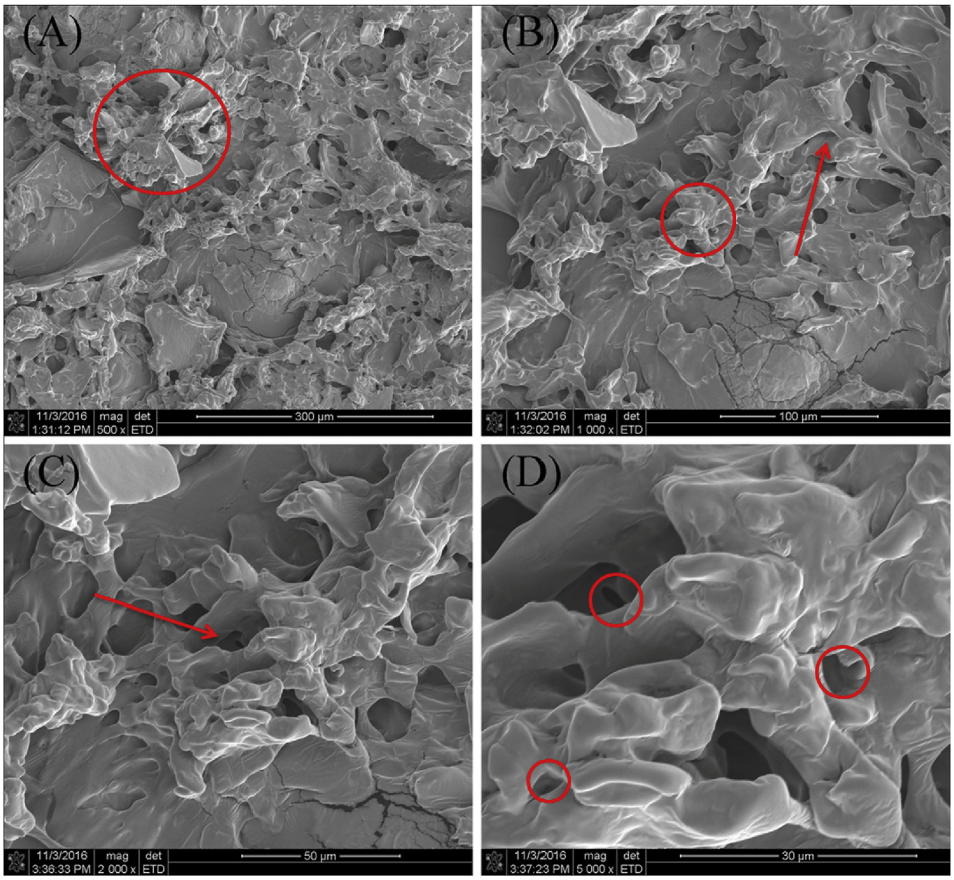

Fig. 7. Field emission scanning electron microscope images of FP20, (A): ×500; (B): ×1000; (C): ×2000; (D): ×5000.

hydrolyze FP20. It was known that enzymes embedded in the small intestinal could hydrolyze some polysaccharides (Woolnough et al., 2008). Zhu et al. (2019a) reported that the molecular weight of *A. heterophyllus* Lam. pulp polysaccharide decreased following *in vitro* intestinal digestion.

3.6.2. Simulated saliva-gastric and saliva-gastric-small intestinal digestion

In vivo, food enters the stomach via the esophagus following digestion in the mouth. However, FP20 was less susceptible to digestion by saliva followed by gastric juices (Table 3): even after 6 h, there was no significant change in its molecular weight. Wang et al. (2019) reported that *Coralline pilulifera* polysaccharide was not digested under simulated saliva-gastric digestion conditions, and that its molecular weight remain unchanged.

By contrast, after passage through the saliva-gastric juice, FP20 also would not be digested by small intestinal juice (Table 3). However, after 6 h incubation, the molecular weight of FP20 was 1.068×10^6 (± 1.910%) g/mol, which was not significantly different to its initial molecular weight. This was in contrast to the results from small intestinal digestion alone, which did change the molecular weight of FP20. It might be that the tightly packed sphere chain conformation results in the dissociation of FP20 during gastric juice digestion but when FP20 is exposed to small intestinal juice, FP20 reaggregation occurs, resulting in no change in its molecular weight. Hakansson et al. (2012) reported large effects on the solubility and aggregation state of β-glucan solutions after digestion *in vitro*. Lovegrove et al. (2017) reported the reaggregation of polysaccharides exposed to small intestinal conditions. This also might be because digestive products resulting from simulated gastric juice digestion are not removed, resulting in inhibition of enzyme activity in the intestinal juice (Minekus et al., 2014).

4. Conclusions

In this study, a novel polysaccharide from *F. margarita* (named FP20) was determined. Based on the results from FT-IR, GC-MS, ^{1}D, and ^{2}D NMR, FP20 was characterized as a type of mannogalactoglucan, comprising →4)-*β-Glcp*-(1 → 2)-*α-Glcp*-(1 → 2)-*α-Galp*-(1 → 4)-*α-Galp*-(1→ bone, and →2)-*α-Galp*-(1→ with a branching point at C_6 of *β-Manp*. Interestingly, there were particular monosaccharide composition ratios and different sugar residues in the side-chains. The chain conformation and surface morphology were studied by AFM and FESEM, which indicated that FP20 had a spherical aggregation, resulting from the entanglement of individual units that were morphed into an aggregated mass. Furthermore, FP20 was susceptible to *in vitro* digestion by small intestinal juice but not by either saliva or gastric juice. However, it was resistant to *in vitro* digestion by either saliva-gastric or

Table 3
Changes in molecular weight of FP20 after digestion.

Time/h	Saliva	Gastric	Small intestinal	Saliva- Gastric	Saliva-Gastric-Small intestinal
2	1.253×10^6 (± 1.579%)	1.284×10^6 (± 1.538%)	8.415×10^5 (± 1.381%)	–	–
4	1.261×10^6 (± 1.778%)	1.157×10^6 (± 2.579%)	3.413×10^5 (± 3.289%)	–	–
6	1.212×10^6 (± 2.972%)	1.099×10^6 (± 1.480%)	3.130×10^5 (± 1.457%)	1.141×10^6 (± 1.862%)	1.068×10^6 (± 1.910%)

saliva-gastric-small intestinal juices. This result might be attributed to its backbone unit and tight, uniform, and spherical chain conformation. This results might provide a theoretical basis for the study of the relationship between structural and functional properties of active polysaccharides.

Declaration of competing interest

The authors declare that they have no known competing financial interests or personal relationships that could have appeared to influence the work reported in this paper.

Acknowledgments

This work was supported by the Project of International Cooperation and Exchanges in Science and Technology of Fujian Agriculture and Forestry University (grant number KXGH17001), the Support Project for Distinguished Young Scholars of Fujian Agriculture and Forestry University (Grant Number xjq201714), the Science and Technology Innovation Project of Fujian Agriculture and Forestry University (Grant number CXZX2017414, CXZX2017018), the Program for Leading Talent in Fujian Provincial University (Grant Number 660160190), and Program for New Century Excellent Talents in Fujian Province University (Grant Number KLA18058A).

References

Capek, P., Kubackova, M., Alfoldi, J., Bilisics, L., Liskova, D., Kakoniova, D., 2000. Galactoglucomannan from the secondary cell wall of *Picea abies L. Karst*. Carbohydr. Res. 329, 635–645.

Chen, C., Zhang, B., Fu, X., You, L.J., Abbasi, A.M., Liu, R.H., 2016. The digestibility of mulberry fruit polysaccharides and its impact on lipolysis under simulated saliva, gastric and intestinal conditions. Food Hydrocolloids 58, 171–178.

Chen, G.J., Xie, M.H., Wan, P., Chen, D., Ye, H., Chen, L.G., Zeng, X.X., Liu, Z.H., 2018a. Digestion under saliva, simulated gastric and small intestinal conditions and fermentation *in vitro* by human intestinal microbiota of polysaccharides from Fuzhuan brick tea. Food Chem. 244, 331–339.

Chen, P.L., You, Q.X., Li, X., Chang, Q., Zhang, Y., Zheng, B.D., Hu, X.K., Zeng, H.L., 2019. Polysaccharide fractions from *Fortunella margarita* affect proliferation of *Bifidobacterium adolescentis* ATCC 15703 and undergo structural changes following fermentation. Int. J. Biol. Macromol. 123, 1070–1078.

Chen, Y.Q., Liu, Y.Y., Sarker, M.M.R., Yan, X., Yang, C.F., Zhao, L.N., Lv, X.C., Liu, B., Zhao, C., 2018b. Structural characterization and antidiabetic potential of a novel heteropolysaccharide from *Grifola frondosa* via IRS1/PI3K-JNK signaling pathways. Carbohydr. Polym. 198, 452–461.

Cheng, H.N., Neiss, T.G., 2012. Solution NMR spectroscopy of food polysaccharides. Polym. Rev. 52, 81–114.

Cilla, A., Gonzalez-Sarrias, A., Tomas-Barberan, F.A., Espin, J.C., Barbera, R., 2009. Availability of polyphenols in fruit beverages subjected to in vitro gastrointestinal digestion and their effects on proliferation, cell-cycle and apoptosis in human colon cancer Caco-2 cells. Food Chem. 114, 813–820.

Colodel, C., Vriesmann, L.C., Petkowicz, C.L.D., 2018. Cell wall polysaccharides from Ponkan Mandarin (*Citrus reticulata* Blanco *cv. Ponkan*) peel. Carbohydr. Polym. 195, 120–127.

Di, T., Chen, G.J., Sun, Y., Ou, S.Y., Zeng, X.X., Ye, H., 2018. In vitro digestion by saliva, simulated gastric and small intestinal juices and fermentation by human fecal microbiota of sulfated polysaccharides from *Gracilaria rubra*. J. Funct. Food. 40, 18–27.

Ding, Y., Yan, Y., Peng, Y., Chen, D., Mi, J., Lu, L., Luo, Q., Li, X., Zeng, X., Cao, Y., 2018. In vitro digestion under simulated saliva, gastric and small intestinal conditions and fermentation by human gut microbiota of polysaccharides from the fruits of *Lycium barbarum*. Int. J. Biol. Macromol. 125, 751–760.

Fan, J.M., Zhang, J.S., Tang, Q.J., Liu, Y.F., Zhang, A.Q., Pan, Y.J., 2006. Structural elucidation of a neutral fucogalactan from the mycelium of *Coprinus comatus*. Carbohydr. Res. 341, 1130–1134.

Feng, L., Yin, J.Y., Nie, S.P., Wan, Y.Q., Xie, M.Y., 2018. Enzymatic purification and structure characterization of glucuronoxylan from water extract of *Cassia obtusifolia* seeds. Int. J. Biol. Macromol. 107, 1438–1446.

Gao, H., Zhang, W.C., Wu, Z.Y., Wang, H.Y., Hui, A.L., Meng, L., Chen, P.P., Xian, Z.J., He, Y.W., Li, H.H., Du, B., Zhang, H.W., 2018. Preparation, characterization and improvement in intestinal function of polysaccharide fractions from okra. J. Funct. Food. 50, 147–157.

Giannotti, M.I., Rinaudo, M., Vancso, G.J., 2007. Force spectroscopy of hyaluronan by atomic force microscopy: from hydrogen-bonded networks toward single-chain behavior. Biomacromolecules 8, 2648–2652.

Gong, L., Zhang, H., Niu, Y.G., Chen, L., Liu, J., Alaxi, S., Shang, P.P., Yu, W.J., Yu, L.L., 2015. A novel alkali extractable polysaccharide from *Plantago asiatic L.* Seeds and its radical-scavenging and bile acid-binding activities. J. Agric. Food Chem. 63, 569–577.

Hakansson, A., Ulmius, M., Nilsson, L., 2012. Asymmetrical flow field-flow fractionation enables the characterization of molecular and supramolecular properties of cereal beta-glucan dispersions. Carbohydr. Polym. 87, 518–523.

He, Y.M., Liu, C.H., Chen, Y.X., Ji, A.C., Shen, Z.L., Xi, T., Yao, Q.S., 2007. Isolation and structural characterization of a novel polysaccharide prepared from *Arca subcrenata Lischke*. J. Biosci. Bioeng. 104, 111–116.

Hou, G.H., Chen, X., Li, J.L., Ye, Z.Y., Zong, S., Ye, M., 2019. Physicochemical properties, immunostimulatory activity of the *Lachnum* polysaccharide and polysaccharide-dipeptide conjugates. Carbohydr. Polym. 206, 446–454.

Humphrey, S.P., Williamson, R.T., 2001. A review of saliva: normal composition, flow, and function. J. Prosthet. Dent 85, 162–169.

Ji, X.L., Zhang, F., Zhang, R., Liu, F., Peng, Q., Wang, M., 2019. An acidic polysaccharide from *Ziziphus Jujuba cv. Muzao*: purification and structural characterization. Food Chem. 274, 494–499.

Li, J., Li, B., Geng, P., Song, A.X., Wu, J.Y., 2017a. Ultrasonic degradation kinetics and rheological profiles of a food polysaccharide (konjac glucomannan) in water. Food Hydrocolloids 70, 14–19.

Li, S., Li, J.H., Zhi, Z.J., Wei, C.Y., Wang, W.J., Ding, T.A., Ye, X.Q., Hu, Y.Q., Linhardt, R.J., Chen, S.G., 2017b. Macromolecular properties and hypolipidemic effects of four sulfated polysaccharides from sea cucumbers. Carbohydr. Polym. 173, 330–337.

Liu, H.F., Gong, F., Wei, F.S., Wu, H., 2018. Artificial simulation of salivary and gastrointestinal digestion, and fermentation by human fecal microbiota, of polysaccharides from *Dendrobium aphyllum*. RSC Adv. 8, 13954–13963.

Liu, W., Wang, H., Yu, J.P., Liu, Y.M., Lu, W.S., Chai, Y., Liu, C., Pan, C., Yao, W.B., Gao, X.D., 2016. Structure, chain conformation, and immunomodulatory activity of the polysaccharide purified from *Bacillus Calmette Guerin* formulation. Carbohydr. Polym. 150, 149–158.

Lovegrove, A., Edwards, C.H., De Noni, I., Patel, H., El, S.N., Grassby, T., Zielke, C., Ulmius, M., Nilsson, L., Butterworth, P.J., Ellis, P.R., Shewry, P.R., 2017. Role of polysaccharides in food, digestion, and health. Crit. Rev. Food Sci. Nutr. 57, 237–253.

Ma, L.S., Chen, H.X., Zhang, Y., Zhang, N., Fu, L.L., 2012. Chemical modification and antioxidant activities of polysaccharide from mushroom *Inonotus obliquus*. Carbohydr. Polym. 89, 371–378.

Minekus, M., Alminger, M., Alvito, P., Ballance, S., Bohn, T., Bourlieu, C., Carriere, F., Boutrou, R., Corredig, M., Dupont, D., Dufour, C., Egger, L., Golding, M., Karakaya, S., Kirkhus, B., Le Feunteun, S., Lesmes, U., Macierzanka, A., Mackie, A., Marze, S., McClements, D.J., Menard, O., Recio, I., Santos, C.N., Singh, R.P., Vegarud, G.E., Wickham, M.S.J., Weitschies, W., Brodkorb, A., 2014. A standardised static in vitro digestion method suitable for food - an international consensus. Food Funct. 5, 1113–1124.

Nie, S.P., Cui, S.W., Phillips, A.O., Xie, M.Y., Phillips, G.O., Al-Assaf, S., Zhang, X.L., 2011. Elucidation of the structure of a bioactive hydrophilic polysaccharide from *Cordyceps sinensis* by methylation analysis and NMR spectroscopy. Carbohydr. Polym. 84, 894–899.

Ognyanov, M., Georgiev, Y., Petkova, N., Ivanov, I., Vasileva, I., Kratchanova, M., 2018. Isolation and characterization of pectic polysaccharide fraction from *in vitro* suspension culture of *Fumaria officinalis L.* Int. J. Polym. Sci. 1–13.

Pedersen, A.M., Bardow, A., Jensen, S.B., Nauntofte, B., 2002. Saliva and gastrointestinal functions of taste, mastication, swallowing and digestion. Oral Dis. 8, 117–129.

Petkova, N., Petrova, I., Ivanov, I., Mihov, R., Hadjikinova, R., Ognyanov, M., Nikolova, V., 2017. Nutritional and antioxidant potential of carob (*Ceratonia siliqua*) flour and evaluation of functional properties of its polysaccharide fraction. J. Pharm. Sci. Res. 9, 2189–2195.

Schroder, R., Nicolas, P., Vincent, S.J., Fischer, M., Reymond, S., Redgwell, R.J., 2001. Purification and characterisation of a galactoglucomannan from kiwifruit (*Actinidia deliciosa*). Carbohydr. Res. 331, 291–306.

Shi, J.J., Zhang, J.G., Sun, Y.H., Xu, Q.X., Li, L., Prasad, C., Wei, Z.J., 2016. The rheological properties of polysaccharides sequentially extracted from peony seed dreg. Int. J. Biol. Macromol. 91, 760–767.

Tang, W., Shen, M.Y., Xie, J.h., Liu, D., Du, M.X., Lin, L.H., Gao, H., Hamaker, B.R., Xie, M.Y., 2017. Physicochemical characterization, antioxidant activity of polysaccharides from *Mesona chinensis* Benth and their protective effect on injured NCTC-1469 cells induced by H_2O_2. Carbohydr. Polym. 175, 538–546.

Tenore, G.C., Campiglia, P., Giannetti, D., Novellino, E., 2015. Simulated gastrointestinal digestion, intestinal permeation and plasma protein interaction of white, green, and black tea polyphenols. Food Chem. 169, 320–326.

Wang, C., Li, W.W., Chen, Z.Q., Gao, X.D., Yuan, G.Q., Pan, Y.X., Chen, H.X., 2018. Effects of simulated gastrointestinal digestion *in vitro* on the chemical properties, antioxidant activity, α-amylase and α-glucosidase inhibitory activity of polysaccharides from *Inonotus obliquus*. Food Res. Int. 103, 280–288.

Wang, H.S., Tang, X., Cheserek, M.J., Shi, Y.H., Le, G.W., 2015. Obesity prevention of synthetic polysaccharides in high-fat diet fed C57BL/6 mice. J. Funct. Food. 17, 563–574.

Wang, K.P., Wang, J., Li, Q., Zhang, Q.L., You, R.X., Cheng, Y., Luo, L., Zhang, Y., 2014. Structural differences and conformational characterization of five bioactive polysaccharides from *Lentinus edodes*. Food Res. Int. 62, 223–232.

Wang, Y.D., Chen, G.J., Peng, Y.J., Rui, Y., Zeng, X.X., Ye, H., 2019. Simulated digestion and fermentation *in vitro* with human gut microbiota of polysaccharides from *Coralline pilulifera*. LWT - Food Sci. Technol. (Lebensmittel-Wissenschaft -Technol.) 100, 167–174.

Wen, S.Y., Zhou, G.H., Song, S.X., Xu, X.L., Voglmeir, J., Liu, L., Zhao, F., Li, M.J., Li, L., Yu, X.B., Bai, Y., Li, C.B., 2015. Discrimination of *in vitro* and *in vivo* digestion products of meat proteins from pork, beef, chicken, and fish. Proteomics 15, 3688–3698.

Woolnough, J.W., Monro, J.A., Brennan, C.S., Bird, A.R., 2008. Simulating human carbohydrate digestion *in vitro*: a review of methods and the need for standardisation.

Int. J. Food Sci. Technol. 43, 2245–2256.
Xue, B.L., Wen, J.L., Xu, F., Sun, R.C., 2012. Structural characterization of hemicelluloses fractionated by graded ethanol precipitation from *Pinus yunnanensis*. Carbohydr. Res. 352, 159–165.
Yang, L.Q., Zhang, L.M., 2009. Chemical structural and chain conformational characterization of some bioactive polysaccharides isolated from natural sources. Carbohydr. Polym. 76, 349–361.
Ye, M., Qiu, T., Peng, W., Chen, W.X., Ye, Y.W., Lin, Y.R., 2011. Purification, characterization and hypoglycemic activity of extracellular polysaccharides from *Lachnum calyculiforme*. Carbohydr. Polym. 86, 285–290.
Yu, Y., Shen, M.Y., Wang, Z.J., Wang, Y.X., Xie, M.Y., Xie, J.h., 2017. Sulfated polysaccharide from *Cyclocarya paliurus* enhances the immunomodulatory activity of macrophages. Carbohydr. Polym. 174, 669–676.
Yu, Z.Y., Liu, L., Xu, Y.Q., Wang, L.B., Teng, X., Li, X.G., Dai, J., 2015. Characterization and biological activities of a novel polysaccharide isolated from raspberry (*Rubus idaeus L.*) fruits. Carbohydr. Polym. 132, 180–186.
Yun, L.Y., Li, D.Z., Yang, L., Zhang, M., 2019. Hot water extraction and artificial simulated gastrointestinal digestion of wheat germ polysaccharide. Int. J. Biol. Macromol. 123, 174–181.
Zeng, H.L., Chen, P.L., Chang, Q., Zheng, B.D., Zhang, Y., 2019. Hypolipidemic effect of polysaccharides from *Fortunella margarita* (Lour.) Swingle in hyperlipidemic rats. Food Chem. Toxicol. 132, 110663.
Zeng, H.L., Chen, P.L., Huang, C.C., Sheng, J.Y., Chang, Q., Zeng, B.D., Zhang, Y., 2017. Structural features and biological activities of bioactive compounds from *Fortunella margarita* (Lour.) Swingle: a review. Chin. J. Struct. Chem. 36, 2123–2132.
Zeng, H.L., Miao, S., Zhang, Y., Lin, S., Jian, Y.Y., Tian, Y.T., Zheng, B.D., 2016. Isolation, preliminary structural characterization and hypolipidemic effect of polysaccharide fractions from *Fortunella margarita* (Lour.) Swingle. Food Hydrocolloids 52, 126–136.
Zeng, H.L., Zhang, Y., Jian, Y.Y., Tian, Y.T., Miao, S., Zheng, B.D., 2015. Rheological properties, molecular distribution, and microstructure of *Fortunella margarita* (Lour.) Swingle polysaccharides. J. Food Sci. 80, 742–749.
Zhang, F., Shi, J.J., Thakur, K., Hu, F., Zhang, J.G., Wei, Z.J., 2017. Anti-cancerous potential of polysaccharide fractions extracted from peony seed dreg on various human cancer cell lines via cell cycle arrest and apoptosis. Front. Pharmacol. 8, 102.
Zhang, T.T., Ye, J.F., Xue, C.H., Wang, Y.M., Liao, W.Z., Mao, L.M., Yuan, M.M., Lian, S., 2018. Structural characteristics and bioactive properties of a novel polysaccharide from *Flammulina velutipes*. Carbohydr. Polym. 197, 147–156.
Zhang, Y., Gu, M., Wang, K.P., Chen, Z.X., Dai, L.Q., Liu, J.Y., Zeng, F., 2010. Structure, chain conformation and antitumor activity of a novel polysaccharide from *Lentinus edodes*. Fitoterapia 81, 1163–1170.
Zhao, C., Gao, L.Y., Wang, C.Y., Liu, B., Jin, Y., Xing, Z., 2016. Structural characterization and antiviral activity of a novel heteropolysaccharide isolated from *Grifola frondosa* again stentero virus 71. Carbohydr. Polym. 144, 382–389.
Zheng, C., Liu, Y.P., Zhou, Q.H., Di, X., 2010. Capillary electrophoresis with non-covalently bilayer-coated capillaries for stability study of allergenic proteins in simulated gastrointestinal fluids. J. Chromatogr. B 878, 2933–2936.
Zhu, K.X., Yao, S.W., Zhang, Y.J., Liu, Q.B., Xu, F., Wu, G., Dong, W.J., Tan, L.H., 2019a. Effects of *in vitro* saliva, gastric and intestinal digestion on the chemical properties, antioxidant activity of polysaccharide from *Artocarpus heterophyllus Lam.* (Jackfruit) Pulp. Food Hydrocolloids 87, 952–959.
Zhu, R.G., Zhang, X.Y., Wang, Y., Zhang, L.J., Zhao, J., Chen, G., Fan, J.G., Jia, Y.F., Yan, F.W., Ning, C., 2019b. Characterization of polysaccharide fractions from fruit of *Actinidia arguta* and assessment of their antioxidant and antiglycated activities. Carbohydr. Polym. 210, 73–84.